

## Article

# Large Transfer of Nitrogen, Silicon and Titanium through Various Thin Mo–Ti/Si and Ti–Mo/Si Bilayer Films Processed in Expanding Microwave Plasma: Formation of Nitrides and Silicides

Isabelle Jauberteau <sup>1,\*</sup>, Richard Mayet <sup>1</sup>, Julie Cornette <sup>1</sup>, Pierre Carles <sup>1</sup>, Denis Mangin <sup>2</sup>, Annie Bessaudou <sup>3</sup>, Jean Louis Jauberteau <sup>1</sup> and Armand Passelergue <sup>3</sup>

<sup>1</sup> Faculté des Sciences et Techniques, Université de Limoges, CNRS, UMR7315, IRCER, CEC, 12 rue Atlantis, F-87068 Limoges, France; richard.mayet@unilim.fr (R.M.); julie.cornette@unilim.fr (J.C.); pierre.carles@unilim.fr (P.C.); jean-louis.jauberteau@unilim.fr (J.L.J.)

<sup>2</sup> Institut Jean Lamour, CNRS, UMR7198, Université de Lorraine, site ARTEM, 2 allée A. Guinier, F-54011 Nancy, France; denis.mangin@univ-lorraine.fr

<sup>3</sup> Faculté des Sciences et Techniques, Université de Limoges, CNRS, XLIM, UMR6172, 123 av. A. Thomas, F-87060 Limoges, France; annie.bessaudou@unilim.fr (A.B.); armand.passelergue@unilim.fr (A.P.)

\* Correspondence: isabelle.jauberteau@unilim.fr; Tel.: +33-58-750-2323

**Abstract:** Silicides and nitrides of transition metals are expected to play a great role in various applications. They can be both considered as metals and ceramics. Their low resistivity and high melting point make them especially promising for super capacitors technology. Thin bilayer films of Mo and Ti are evaporated on Si substrates with various thicknesses and location with respect to the Si substrate. They are exposed to expanding plasma using (Ar-31%N<sub>2</sub>-6%H<sub>2</sub>) gas mixtures, which promotes the chemical reactions on the surface of the bilayer films. Because of the intensive diffusion of elements such as Si and Ti, which compete with the diffusion of nitrogen into the surface layers, various thin films of nitrides and silicides form, depending on the location of Mo and Ti films relative to Si substrates. Results are analyzed in light of thermodynamic and kinetic considerations and especially the strong reactivity of Ti towards oxygen and silicium compared with Mo. The large diffusion of Si through Mo–Ti/Si bilayer films prevents the formation of nitrides, whereas a film of Mo, only 50 nm thick, prevents the formation of silicides in Ti–Mo/Si bilayer films, which promotes the formation of TiN from TiO<sub>2</sub> and nitrogen due to the reducing and nitriding effect of plasma.

**Keywords:** expanding plasma; Mo–Ti thin bilayer films; silicides; nitrides; composition; structure; nitriding process



**Citation:** Jauberteau, I.; Mayet, R.; Cornette, J.; Carles, P.; Mangin, D.; Bessaudou, A.; Jauberteau, J.L.; Passelergue, A. Large Transfer of Nitrogen, Silicon and Titanium through Various Thin Mo–Ti/Si and Ti–Mo/Si Bilayer Films Processed in Expanding Microwave Plasma: Formation of Nitrides and Silicides. *Coatings* **2023**, *13*, 1787. <https://doi.org/10.3390/coatings13101787>

Academic Editor: Heping Li

Received: 18 September 2023

Revised: 6 October 2023

Accepted: 10 October 2023

Published: 18 October 2023



**Copyright:** © 2023 by the authors. Licensee MDPI, Basel, Switzerland. This article is an open access article distributed under the terms and conditions of the Creative Commons Attribution (CC BY) license (<https://creativecommons.org/licenses/by/4.0/>).

## 1. Introduction

The attractive physical and chemical properties of transition metal silicides (TMS) make them very interesting for a wide range of applications. They exhibit high temperature stabilities, low resistivity, chemical compatibilities and low Schottky barrier heights. Among TMS, TiSi<sub>2</sub> has the lowest resistivity, 14–17 μΩ·cm. Therefore, it is used as contacts and interconnects on Si metal oxide semiconductor (MOS) devices [1,2]. The resistivity of MoSi<sub>2</sub> is approximately 40 μΩ·cm [3]. Its melting point is very high (2030 °C). Therefore, in addition to applications for MOS devices, MoSi<sub>2</sub> is used for its great antioxidant properties at high temperatures [4]. Moreover, the thermal conductivity of thin solid films of Mo–Si nanocrystals is lower than that of films of Si nanocrystals, which makes them very attractive for high-efficiency thermoelectric materials [5]. The hexagonal structure of MoSi<sub>2</sub> exhibits semiconducting properties with a narrow band gap of 0.035 eV. Thin amorphous films of molybdenum silicides are potential candidates for single-photon detectors. Recent

temperature-dependent resistance and magneto resistance measurements have detected electronic transport of the Mott variable hopping conductivity mechanism [6].

The addition of nitrogen during the formation of  $\text{TiSi}_2$  plays a conspicuous role in improving the properties. Rapid thermal annealing in nitrogen ambient prevents the lateral growth of  $\text{TiSi}_2$ , which induces shorting in complementary MOS (cMOS) devices during Ti–Si reactions [7–9]. In the same way, the barrier height of  $\text{TiSi}_x/\text{Si}$  Schottky diodes is reduced by 80 meV, which results in approximately 15% of self-power consumption saving, owing to the diffusion of nitrogen into  $\text{TiSi}_x$  [10].

Transition metal nitrides (TMN) exhibit unusual physical and chemical properties because the structure consists of a mixture of metallic, covalent and ionic bonding. Various structures with disordered N atoms and strong deviations from stoichiometry attributed to N vacancies, interstitials and more recently to metal vacancies, have been evidenced [11–13]. Similar to TMS, their physical and chemical properties such as thermal and chemical stability, corrosion resistance, extreme hardness, high melting point, low electrical resistivity and thermal resistance make them suitable for a wide number of applications. Among all TMN, TiN exhibits a melting point of 2947 °C, which is higher than those usually found in ceramics such as AlN,  $\text{Al}_2\text{O}_3$  or  $\text{Si}_3\text{N}_4$ . The electrical resistivity of TiN is 30  $\mu\Omega\cdot\text{cm}$  and can be compared to the metals [14]. Therefore, it is used as a MEMS electrode in cMOS technology and Schottky diodes [15,16]. On the other hand, the electrical resistivity of  $\text{Mo}_2\text{N}$  is only 19.8  $\mu\Omega\cdot\text{cm}$  [12]. The metastable MoN phase of the NaCl-B1-type structure is expected to have the highest superconducting temperature among all refractory carbides and nitrides. Molybdenum nitrides are also very active for adsorption and catalytic reactions [17–19].

Ti and Mo nitrides are promising candidates as electrode materials for supercapacitors [20,21]. It is well known that titanium exhibits high reactivity towards oxygen and the combination of oxides and nitrides is promising to develop high-performance supercapacitor electrode materials [20,22]. The role of oxygen vacancies and the growth of a  $\text{TiO}_x$  layer on enhancing capacitance properties have especially been evidenced in TiN electrodes. Moreover, the combination of two or three transition metal layers allows the properties of components to be greatly enhanced. A Mo–Ti buffer layer is introduced in n-type skutterudite (SKD), a  $\text{Yb}_{0.3}\text{Co}_4\text{Sb}_{12}$  matrix of thermoelectric joints which exhibit an excellent stability of the contact resistivity [23] by decreasing the interdiffusion between Ti and matrix. The  $\text{MoN}_x/\text{TiN}$  system forms a stable electric double-layer capacitance in alkaline media [20,24,25].

TMS are synthesized during thermal annealing of TM thin films coated on Si substrates, whereas TMN films are mainly synthesized in  $\text{N}_2$  or  $(\text{Ar-N}_2)$  gas using reactive sputtering by means of direct current, radio-frequency or magnetron discharges. TMN exhibit various stoichiometry, crystallized and amorphous structures, which are obtained by varying the temperature and the nitrogen pressure in the process. Other processes such as ion implantation, pulsed laser irradiation, and atomic layer deposition are carried out to deposit thin TMN films onto substrates [12–14,26].

In our laboratory, thin TMN films are prepared by means of plasma-enhanced chemical vapor deposition using microwave discharge. The high degree of ionization and dissociation makes microwave plasma very attractive compared with other types of electrical excitations. The expanding plasma process promotes reactions on the surface of metal films.  $(\text{Ar-N}_2\text{-H}_2)$  plasma mainly consists of  $\text{Ar}^+$  ions and reactive species such as  $\text{NH}_x$  and H atoms, which reduce the remaining passive layers as oxides and prevent the formation of oxides during treatment, thus improving nitrogen diffusion into the surface layers. Mo and Ti nitrides have been successfully synthesized from thin Mo and Ti films exposed to  $(\text{Ar-N}_2\text{-H}_2)$  expanding plasma activated by microwaves of 2.45 GHz [12,27,28]. Only 20 min of treatment produces MoN thin films, 500 nm thick, at low power and low temperature. Mo–Ti bilayers consisting of Mo and Ti films, 250 nm thick each, deposited on Si wafers, respectively, have been successfully nitrated and resulted in the formation of faceted grains of TiN of nanometric sizes on the bilayer surface [29]. The aim of this work is to investigate the formation and the crystallization of compounds such as silicides

and nitrides in four Mo–Ti bilayer thin films of different thicknesses and locations with respect to the Si substrate, heated up to 873 K and exposed to (Ar–N<sub>2</sub>–H<sub>2</sub>) plasma. The work is especially focused on the diffusion of nitrogen from the plasma into the surface layers and the diffusion of various elements through the bilayer films, which results in the simultaneous formation and crystallization of silicides and nitrides. The analysis of the results includes thermodynamic and kinetic considerations. It is expected to throw a light upon the formation and crystallization of nitrides and silicides in Mo–Ti bilayer thin films processed in expanding plasma.

## 2. Materials and Methods

### 2.1. Mo–Ti/Si and Ti–Mo/Si Bilayer Films

A series of four Mo–Ti bilayer films, MoTi1, TiMo1, TiMo2 and TiMo3, are coated on Si (100) wafers. Various thicknesses and locations of Mo and Ti thin films relative to the Si substrate are obtained from successive evaporation of pure Mo and Ti cylinders and pellets (99.95%) on Si wafers biased at  $-400$  V and heated at  $400$  °C in Ar gas at a pressure of  $0.5$  Pa. These conditions allow the adhesion of the films on substrates to be improved.

MoTi1 consists of a Ti film,  $250$  nm thick, coated on Si wafer and capped with a Mo film,  $100$  nm thick.

TiMo1 consists of a Mo film,  $50$  nm thick, coated on Si wafer and capped with a Ti film,  $250$  nm thick.

TiMo2 consists of a Mo film,  $100$  nm thick, coated on Si wafer and capped with a Ti film,  $100$  nm thick.

TiMo3 consists of a Mo film,  $250$  nm thick, coated on Si wafer and capped with a Ti film,  $50$  nm thick.

The samples (approximately  $1$  cm<sup>2</sup>) are then cut from the wafers with a diamond tip.

### 2.2. Thermochemical Treatment by Means of an Expanding Plasma Process

The samples are placed on the heating substrate holder at  $12.5$  cm from the center of the discharge in the plasma reactor (Figure 1).

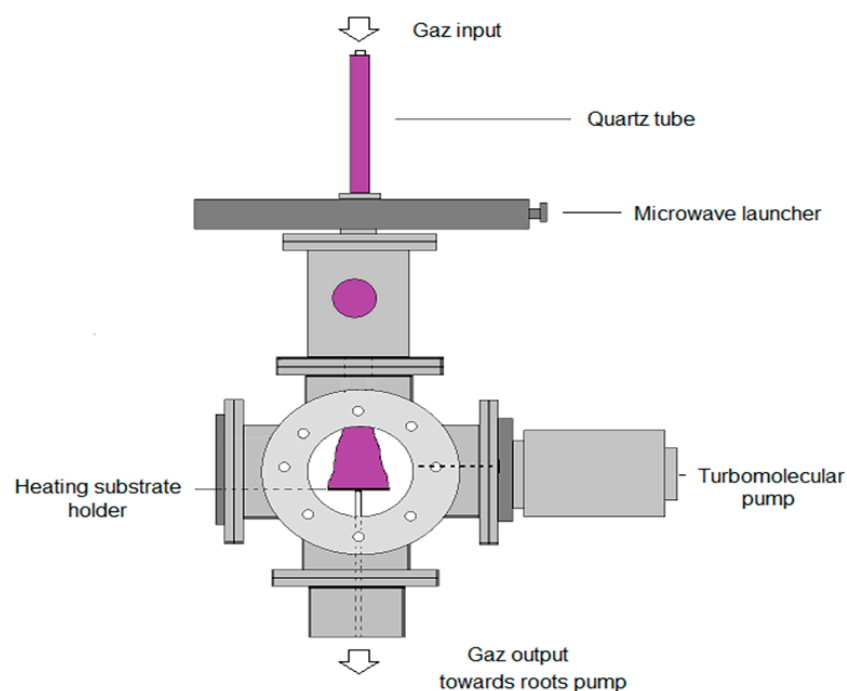


Figure 1. Experimental setup.

The reactor consists of a fused silica tube (external and internal diameter of 24 and 20 mm, respectively) passing through a surface wave launcher where a microwave discharge of 2.45 GHz is produced using a power supply SAIREM GMP 12 kE operating up to 1.2 kW. A turbo molecular pump maintains a base pressure of  $10^{-5}$  Pa and the total pressure of 0.13 kPa is kept constant using an Alcatel roots blower pump ( $70\text{--}700\text{ m}^3\cdot\text{h}^{-1}$ ) during the experiments. After heating to the required temperature of 400, 600 or 800 °C, the (Ar-31%N<sub>2</sub>-6%H<sub>2</sub>) gas mixture is introduced and the discharge is produced with a power of 500 W. The composition of the plasma allows an expanding plasma producing a large amount of NH<sub>x</sub> species to be obtained. The experiments are run for 0.5 h, 1.5 h or 3 h. Subsequent to nitridation, the substrates are allowed to cool to room temperature in the reactor. The plasma is produced by a surface wave which propagates in the quartz tube along the external surface of the plasma. It is expanded out, forming a bright cone from the quartz tube exit up to the surface of the substrate under conditions of large density of electrons which depends on the density of collisions and the microwave frequency. The density of electrons measured along the discharge axis ranges between 0.03 and  $0.15 \times 10^{16}\text{ m}^{-3}$  and their energy ranges between 0.51 and 1.37 eV. The density of Ar is approximately  $2 \times 10^{22}\text{ m}^{-3}$  and is 100 times larger than that of NH<sub>3</sub> and NH<sub>2</sub> radicals and  $10^3$  and  $10^4$  larger than that of NH and N radicals. The flux of Ar<sup>+</sup> ions is approximately  $7 \times 10^{18}\text{ m}^2\cdot\text{s}^{-1}$ . The ion energy at the sheath is only approximately 0.1 eV, so the sputtering effect of the impinging energetic ions which is unavoidable in other processes reduces passive layers on the surface or the films is trifling. The remaining passive oxides or carbides are reduced by the hydrogen species, NH<sub>x</sub> radicals and/or H atoms produced in the plasma [30].

### 2.3. Investigations of Mo–Ti/Si and Ti–Mo/Si Bilayer Films

Various means of investigation such as X-ray diffraction (XRD), Raman spectroscopy, secondary ion mass spectrometry (SIMS), scanning electron microscopy (SEM), transmission electron microscopy (TEM), selected area electron diffraction (SAED) and nano-probe energy dispersive spectrometry (EDS) are conducted in order to determine the phase composition and crystalline structure of the Mo–Ti bilayer films as well as the morphology of the surface, the microstructure and the elemental composition.

#### 2.3.1. X-ray Diffraction Measurements

XRD analysis are carried out in the Bragg Brentano geometry on a D8 Advance Bruker diffractometer operating using monochromatic CuK $\alpha$ 1 radiation and a Lynx-eye position sensitive detector ( $3.4^\circ$  for fast acquisition). A Bruker “D8 discover” diffractometer equipped with a parabolic multilayer G $\ddot{o}$ bel mirror, a two-reflection asymmetrically cut Ge(220) monochromator (Cu K $\alpha$ 1 radiation,  $\lambda = 0.15406\text{ nm}$ ) as primary optics and a linear position sensitive detector (“Lynx Eye”) is used to obtain some grazing angle (GA-XRD) patterns.

#### 2.3.2. Raman Spectroscopy

Raman spectroscopy is performed by means of an InVia Reflex Renisha. The spectra are recorded using a  $\times 100$  objective and a 532 nm wavelength excitation with a power of 4 MW on samples.

#### 2.3.3. Secondary Ion Mass Spectrometry Measurements

SIMS experiments are carried out in a CAMECA IMS 7F spectrometer using cesium ions (Cs<sup>+</sup>) with a primary beam voltage and intensity of 5 kV and 25 nA, respectively. The primary beam is scanned over an area of  $200 \times 200\ \mu\text{m}^2$ . The results are normalized with respect to the cesium signal. This method has been found to have high sensitivity and excellent separation power. However, quantitative analysis may be conducted through relative measurements by adding a calibration factor for most elements. The detection of CsM<sup>+</sup> or CsCsM<sup>+</sup> secondary ions (M is the measured element) prevents matrix effects

since these molecules which are formed on the surface of the sample are not bounded to the matrix.

#### 2.3.4. Scanning and Transmission Microscopy and Energy Dispersive Spectrometry

SEM surface micrographs as well as sample cross-section preparation are obtained with a MEB-FIB ZEISS XB 550 model (GmbH, Oberkochen, Germany) microscope equipped with a focused ion beam system operating with Ga ions for cross-section preparation. The voltage and the current of the ion beam are gradually decreased from 30 kV and 7  $\mu$ A to 5 kV and 10 pA, respectively, during the preparation.

The TEM, SAED and EDS studies are performed in a 2100F JEOL microscope (Tokyo, Japan) at an accelerating voltage of 200 kV.

### 3. Results

#### 3.1. As-Received Mo–Ti/Si and Ti–Mo/Si Bilayer Thin Films

##### 3.1.1. Crystalline Structure Analysis

The X-ray diffraction pattern (a) in Figure 2 corresponding to the untreated MoTi1 bilayer film mainly displays the most intense reflection of the (101) atomic planes at a  $2\theta$  Bragg angle of  $40.17^\circ$  and other weak reflections corresponding to the (002) and (100) atomic planes at  $38.42^\circ$  and  $35.09^\circ$ , all belonging to the pure  $\alpha$  phase of Ti of hexagonal structure (JCPDS card n° 00-044-1294). Mo is only displayed as a shoulder on the larger Bragg angle side of the (101) diffraction line of  $\alpha$ Ti, and as a tiny feature at  $2\theta = 58.6^\circ$ , which corresponds to the (110) and (200) atomic planes of the pure Mo of the body-centered cubic structure (JCPDS card n° 00-042-1120), respectively. The sharp peak at  $2\theta = 33^\circ$  corresponds to the forbidden reflection of the Si substrate [31].

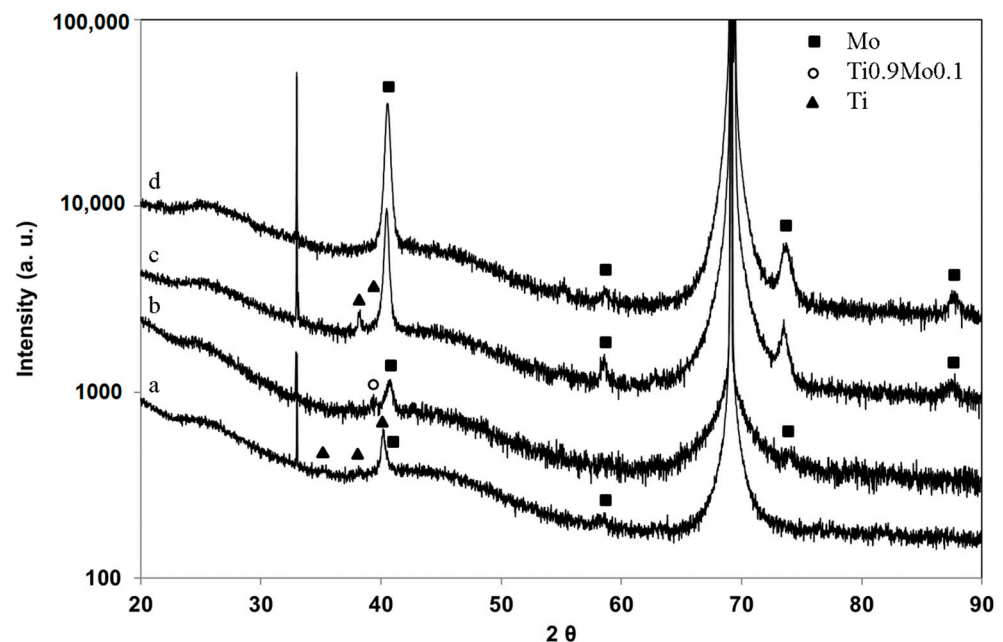


**Figure 2.** X-ray diffraction patterns of as-deposited Mo–Ti bilayer films, MoTi1 (a), TiMo1 (b), TiMo2 (c) and TiMo3 (d).

In contrast, the hexagonal phase of pure Ti is not clearly identified on the diffraction pattern (b) in Figure 2 corresponding to the untreated TiMo1 bilayer film. The most intense reflection line at  $2\theta = 41.05^\circ$  is assigned to the (110) atomic planes of pure Mo, slightly shifted towards larger Bragg angles, which would result in the occurrence of stresses in the Mo film. Large shifts towards larger Bragg angles have been observed on Mo subjected to shock compression [32]. Tiny peaks are identified at approximately  $2\theta = 39^\circ$ . Such values are assigned to the formation of the  $\beta$  phase of Ti of cubic structure. It is worth noting that

Ti can form complete solid solutions with Mo, which promotes the stability of the  $\beta$  phase of the body-centered cubic structure as  $\text{Ti}_{0.9}\text{Mo}_{0.1}$  (JCPDS card n° 04-018-6034) with the most intense (110) reflection line at  $2\theta = 39.08^\circ$ , in contrast with the  $\alpha$  phase of hexagonal structure. More details are given in [29,33–36]. The diffraction pattern (c) in Figure 2 corresponding to the  $\text{TiMo}_2$  bilayer film displays the features of pure Ti of hexagonal structure as well as those of pure Mo. The most intense (101) peak of Ti is displayed as a shoulder on the lower Bragg angle side of the (110) most intense reflection line of Mo. Since Ti is lighter than Mo, its reflection lines are much less intense. Regarding the  $\text{TiMo}_3$  bilayer film, only Mo is identified owing to the very small thickness of the Ti layer (Figure 2 (d)). The tiny peak at approximately  $55^\circ$  is unidentified.

### 3.1.2. Diffusion of Elements

In what follows, the various interfaces between the Mo and Ti films and the Si substrate as well as the location of Mo, Ti, Si, and O elements in  $\text{MoTi}_1$  and  $\text{TiMo}_3$  bilayer films before they are processed are investigated by SIMS. The Ti–Si and Mo–Ti interfaces in the  $\text{MoTi}_1$  bilayer film are clearly displayed in Figure 3.

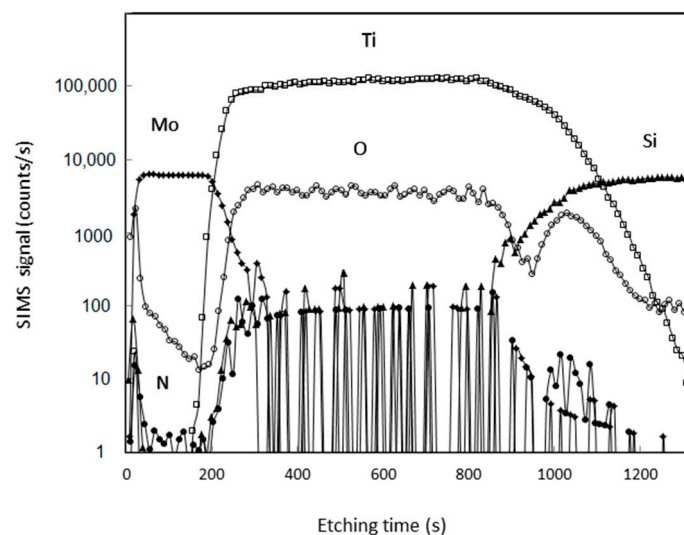


**Figure 3.** SIMS depth profiles of as-deposited  $\text{MoTi}_1$  bilayer film.

Owing to a start of Si and Ti diffusion through the Ti–Si interface during the evaporation of Ti on Si substrates at  $400^\circ\text{C}$ , the Ti–Si interface is broader than the Mo–Ti interface, which is well identified. Moreover, the apparent shift of the hump of the O signal corresponding to the  $\text{SiO}_2$  thin layer which remains at the surface of the Si substrate shows that Si is the main diffusing element as it is usually reported [37]. Because of the great reactivity of Ti towards oxygen, the intensity of the oxygen signal is high in the whole Ti film thickness compared with the low oxygen amount in the Mo film. The enthalpy of formation of  $\text{TiO}_2$  is  $-944\text{ kJ}\cdot\text{mol}^{-1}$  [38] is far lower than those of  $\text{MoO}_2$  and  $\text{MoO}_3$ ,  $-598.94$  and  $-745.05\text{ kJ}\cdot\text{mol}^{-1}$  at 300 K, respectively [39].

In contrast with the  $\text{MoTi}_1$  bilayer film, Si does not diffuse through the Si–Mo interface in  $\text{TiMo}_3$ , no shift of the O signal hump corresponding to  $\text{SiO}_2$  is displayed.

However, a strong Mo and Ti interdiffusion occurs in the  $\text{TiMo}_3$  bilayer film during the evaporation of the Ti film on the Mo film, since Ti diffuses into the whole Mo film passing through the Mo–Si interface up to the Si substrate and Mo slightly diffuses towards the surface (Figure 4) Because of the great reactivity of Ti, the amount of O and N contaminants are higher in the Ti film located at the surface of  $\text{TiMo}_3$  than in the Mo film located at the surface of  $\text{MoTi}_1$ .

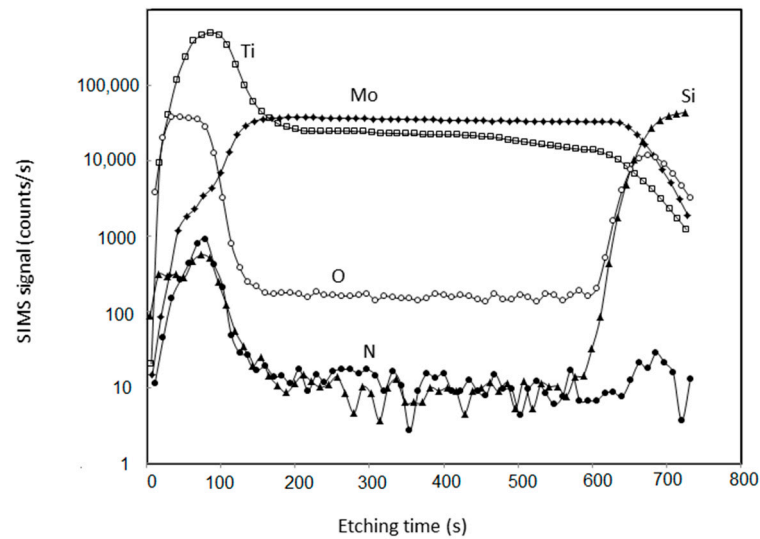


**Figure 4.** SIMS depth profile of as-deposited TiMo3 bilayer film.

### 3.2. Mo–Ti and Ti–Mo Bilayer Films Exposed to (Ar-31%N<sub>2</sub>-6%H<sub>2</sub>) at 600 °C

#### 3.2.1. Crystalline Structures

##### XRD Investigations

A 1 h 30 min exposure of MoTi1 heated at 600 °C in (Ar-31%N<sub>2</sub>-6%H<sub>2</sub>) plasma results in the formation of well-crystallized C54TiSi<sub>2</sub> of face-centered orthorhombic structure (JCPDS card n° 00-035-0785) since the most intense (311), (040), (022) and (331) reflection lines located at 2θ of 39.11°, 42.23°, 43.18° and 49.70°, respectively, are very sharp (Figure 5 (a)). The (111), (220), (351), (620) and (602) diffraction peaks of lower intensity at 23.81°, 30.05°, 67.24°, 71.93° and 80.26° are also identified.

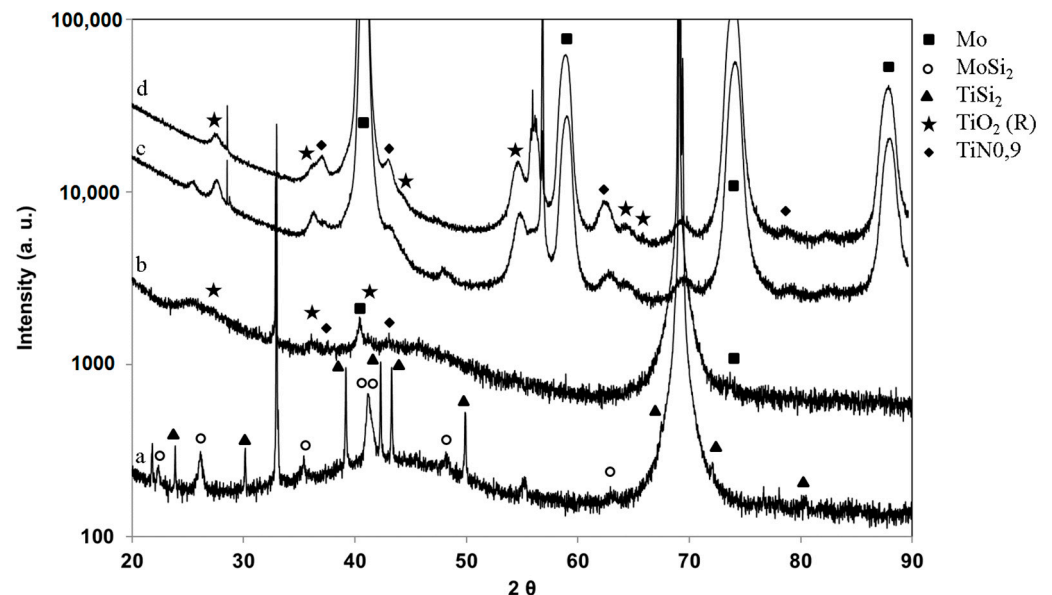


**Figure 5.** Conventional X-ray diffraction patterns of Mo–Ti bilayer films heated at 600 °C and processed in (Ar-31%N<sub>2</sub>-6%H<sub>2</sub>) plasma for 90 min, MoTi1 (a) and TiMo1 (b). Grazing angle X-ray diffraction of TiMo3 bilayer film heated at 600 °C and processed in (Ar-31%N<sub>2</sub>-6%H<sub>2</sub>) plasma for 30 min (c) and 90 min (d).

The preferred orientation of crystallites along the [040] direction is assigned to the occurrence of compressive stresses. The elastic constants are higher in the [010] direction [40]. The other diffraction lines at 2θ = 22.29°, 26.13°, 35.38°, 41.19°, 41.55°, 48.25°, 63.02° and

63.29° correspond to the (100), (101), (102), (003), (111), (112), (203) and (211) atomic planes of the  $\beta$  phase of  $\text{MoSi}_2$  of hexagonal structure, respectively (JCPDS card n° 04-018-0302). The formation of the C49 metastable phase of  $\text{TiSi}_2$  (JCPDS card n° 04-002-1352) cannot be ruled out. Owing to the small size of the crystallites compared with that of  $\text{C54TiSi}_2$ , the reflection lines are less intense. The diffraction peak at approximately 55° is unidentified. The intensity and the broadening of the diffraction line at  $2\theta$  of approximately 41.2° is due to the overlapping of the most intense (111) and the (003) diffraction lines at  $2\theta$  of 41.55° and 41.19° of  $\text{MoSi}_2$ , respectively, as well as the most intense (131) line of the C49 metastable phase of  $\text{TiSi}_2$  located at  $2\theta = 41.15^\circ$ . These results will be confirmed by Raman spectroscopy measurements, in the next section.

Because of the great reactivity of Ti, the Ti–Si reaction is very complex and various Ti silicides are synthesized at a temperature of approximately 500 °C from an extensive intermixing at the Ti film–Si substrate interface [7,27,41]. The strong interdiffusion of Si and Ti has also been identified before the silicide is formed in thin Ti films, 40 nm thick, coated on Si at temperatures ranging between 300 and 400 °C. The disordered structure is made of Si, Ti and O [37]. Si is usually reported to be the dominant diffusing species. This result is confirmed by our previous SIMS measurements. Two mechanisms resulting in the formation of Ti silicides have been identified [41] and references herein. The first one is the diffusion of Si into Ti grain boundaries and the formation of fine-grained crystallites of composition close to  $\text{TiSi}$ . The second one is an interfacial reaction and the formation of an amorphous or a very fine grained silicide layer which grows by diffusion of Si into the Ti film up to saturation which is the start of crystallization. Owing to kinetic factors as well as the state of Si substrate (amorphous or crystallized), various precursors of the  $\text{C54TiSi}_2$  phase are reported in the literature, such as  $\text{TiSi}$ ,  $\text{C49TiSi}_2$ ,  $\text{Ti}_5\text{Si}_3$ ,  $\text{Ti}_5\text{Si}_4$ . They turn into  $\text{C54TiSi}_2$  at higher temperatures. In contrast with our previous results obtained from pure Ti thin films processed under the same experimental conditions [27], the C49 and  $\text{C54TiSi}_2$  phases coexist in our present work. It will be confirmed by Raman spectroscopy measurements.

Among Ti–Mo/Si bilayer films consisting of Mo film capped with a Ti film heated at 600 °C and processed in ( $\text{Ar-31\%N}_2\text{-6\%H}_2$ ) plasma for 1 h 30 min, the first signs of the crystallization of TiN using XRD with conventional Bragg–Brentano geometry investigations are only observed in  $\text{TiMo1}$  (Figure 5 (b)). The tiny (110), (101) and (111) diffraction lines of the rutile phase of  $\text{TiO}_2$  at Bragg angles of approximately 28°, 35.7° and 41.09° (JCPDS card n° 00-021-1276), the tiny peaks of TiN of cubic structure which correspond to the most intense (111) and (200) reflection lines at Bragg angles of 36.69° and 42.62° (JCPDS card n° 04-004-2917) as well as the most intense (110) diffraction peak of pure Mo are identified. Owing to the strong reactivity of Ti towards oxygen, the Ti film consists of oxides of amorphous structure which crystallizes at 600 °C with the structure of the rutile phase. In contrast with  $\text{MoTi1}$ , where Si diffuses from the Si substrate up to the surface leading to the formation of Ti and Mo silicides, the Mo underlayer, 50 nm thick, forms a barrier of diffusion to Si, preventing the formation of Mo and Ti silicides. Therefore, the formation of TiN at 600 °C from the Ti film coated on Mo is possible in contrast with pure Ti films coated on Si substrates, where TiN only starts to crystallize at 800 °C from  $\text{TiSi}_2$  [27]. With regard to  $\text{TiMo2}$  and  $\text{TiMo3}$ , the small thickness of the Ti film does not allow any Ti compounds to be identified by conventional XRD measurements. Only pure Mo is displayed. Since pure Ti has been identified in the pattern of the as received  $\text{TiMo2}$ , Ti is expected to turn into amorphous or ill-crystallized TiN. Some experiments using grazing angle XRD (GA-XRD) have been performed on  $\text{TiMo3}$  processed for 30 and 90 min. to overstep the limit of detection of conventional XRD (Figure 5 (c) and (d), respectively). The reflection lines of TiN and those of the rutile phase of  $\text{TiO}_2$  are clearly displayed in Figure 5 (c) and (d). It is worth noting that the  $\text{TiO}_2$  turns into TiN during the nitridation process since the amount of TiN and  $\text{TiO}_2$  increases and decreases with increasing treatment duration, respectively. However, the formation of Ti oxynitrides cannot be ruled out. The broad feature consisting

of a group of diffraction lines at  $2\theta$  of approximately  $56^\circ$  (Figure 5 (d)) is unidentified as well as the small peaks at approximately  $25.5^\circ$  and  $48^\circ$  (Figure 5 (c)).

### Raman Spectroscopy Investigations

All Raman spectra corresponding to MoTi1, TiMo1, TiMo2 and TiMo3 bilayer films processed in (Ar-31%N<sub>2</sub>-6%H<sub>2</sub>) plasma at 600 °C are well structured and display numerous bands including very sharp peaks and rather broad structures of low intensity.

Raman spectroscopy, which reflects the vibrational bands of the material, is sensitive to disorder. In contrast with crystalline structures, amorphous or disordered structures display broad Raman features of rather low intensities [37].

The most sharp and very intense Raman bands located at wave numbers of 214, 259 and 395 cm<sup>-1</sup> and identified in MoTi1 processed at 600 °C for 1 h 30 min are assigned to well-crystallized  $\beta$ MoSi<sub>2</sub> of hexagonal structure (Figure 6 (a)), the weak and rather broad band at 414 cm<sup>-1</sup> also belongs to MoSi<sub>2</sub> and is usually not very intense [42]. The well-crystallized C54TiSi<sub>2</sub> compound is only identified with the peak at 234 cm<sup>-1</sup> of low intensity. The other peaks are overlapped by the intense Raman features corresponding to  $\beta$ MoSi<sub>2</sub>.

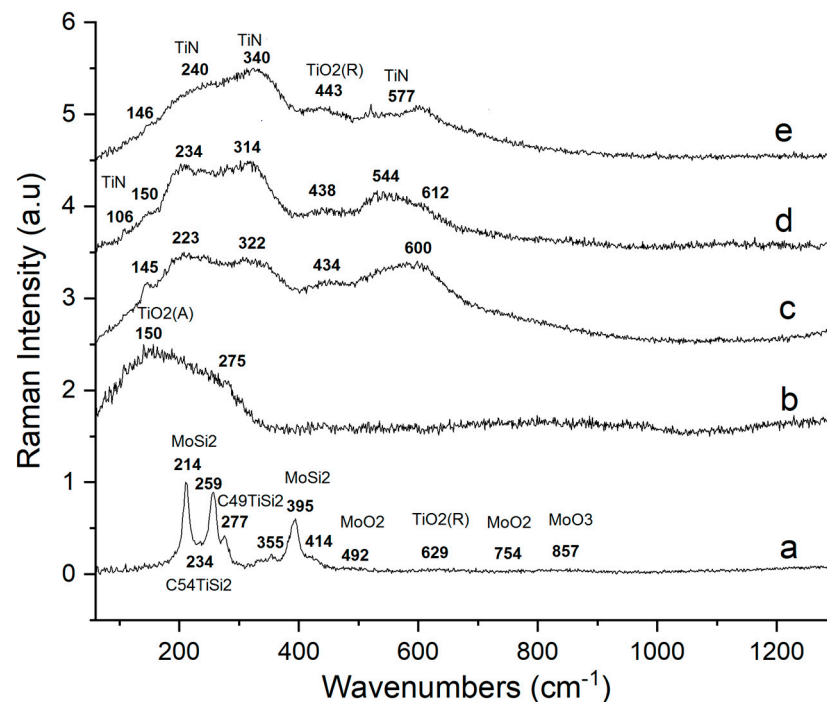


**Figure 6.** Raman scattering spectra of Mo–Ti bilayer films. MoTi1 heated at 600 °C (a) and 500 °C (b), respectively, and processed in (Ar-31%N<sub>2</sub>-6%H<sub>2</sub>) plasma for 90 min (a), TiMo1, TiMo2 and TiMo3 heated at 600 °C and processed in (Ar-31%N<sub>2</sub>-6%H<sub>2</sub>) plasma for 90 min (c), 30 min (d) and 30 min (e), respectively.

The calculated Raman spectra of C54TiSi<sub>2</sub> and  $\beta$ MoSi<sub>2</sub> display nine active Raman bands, respectively—1 A<sub>g</sub>, 3 B<sub>1g</sub>, 3 B<sub>2g</sub> and 2 B<sub>3g</sub> vibrational modes have been determined for C54TiSi<sub>2</sub> [43] and 1 A<sub>1</sub>, 4 degenerate E<sub>1</sub> and 4 degenerate E<sub>2</sub> modes have been determined for MoSi<sub>2</sub> [42]. Regarding TiSi<sub>2</sub>, B<sub>1g</sub> and A<sub>g</sub> at 210 and 250 cm<sup>-1</sup> are the most intense modes, whereas the intensity of the B<sub>1g</sub> modes at 330 and 430 cm<sup>-1</sup> is low, the B<sub>2g</sub> and B<sub>3g</sub> modes are too weak to be observed for polycrystalline TiSi<sub>2</sub>. Since the intense A<sub>g</sub> Raman mode at 234 cm<sup>-1</sup> is identified as a tiny peak in the Raman spectrum (a) in Figure 6, the surface layer, which is expected to mainly consist of  $\beta$ MoSi<sub>2</sub>, could weaken the Raman emission arising from TiSi<sub>2</sub>. A similar effect has been observed in the case of a MoSi<sub>2</sub> layer coated with a TiN layer in our previous work. The surface layer of TiN was

sufficient to block any Raman emissions from MoSi<sub>2</sub> [29]. At higher wave numbers, from approximately 490 cm<sup>-1</sup>, the series of broad spectral features of low intensity correspond to ill-crystallized and/or disordered oxides. The bands at 492 and 754 cm<sup>-1</sup> correspond to the most intense vibrational bands of MoO<sub>2</sub> and that identified at 857 cm<sup>-1</sup> is the most intense Raman band of MoO<sub>3</sub> [44]. One of the two most intense Raman bands of the rutile phase of TiO<sub>2</sub> is also seen at 629 cm<sup>-1</sup>, whereas the other one overlaps the Raman feature of MoSi<sub>2</sub> at 414 cm<sup>-1</sup> [45]. In comparison, the Raman spectrum (b) in Figure 6 obtained from MoTi1 processed under the same experimental conditions but at lower temperatures, only displays the oxide compounds and especially the most intense vibrational band of the anatase phase of TiO<sub>2</sub> at 150 cm<sup>-1</sup> and a less intense broad band at approximately 500 cm<sup>-1</sup>. These results agree with those reported in [45], i.e., the anatase phase turns into the rutile phase with increasing temperature.

The formation of TiN in TiMo1, TiMo2 and TiMo3 bilayer films processed for 1 h 30 min, 30 min and 30 min, respectively, is clearly evidenced in the range of wave numbers between 220 and 240 cm<sup>-1</sup>, 310 and 325 cm<sup>-1</sup> and between 570 and 600 cm<sup>-1</sup> on the corresponding Raman spectra (c), (d) and (e) in Figure 6, respectively. These results confirm those which have been obtained by grazing XRD measurements. TiN forms and crystallizes from Ti and/or TiO<sub>2</sub>, which react with nitrogen produced in the plasma.

Because of the presence of the inversion symmetry in perfect stoichiometric compounds of B1 structure of NaCl type, a first-order Raman spectrum is not possible. However, TiN contains both metal and nitrogen vacancies even in the stoichiometric structure which reduces its effective symmetry. Therefore, a first-order Raman scattering is expected for TiN [14,46,47]. The vibration of the heavy Ti ions near N vacancies induces Raman scattering in the acoustic frequency range (200–350 cm<sup>-1</sup>) whereas the light N ions near Ti vacancies induce Raman scattering in the optical frequency range (500–600 cm<sup>-1</sup>) [14,46]. The Raman band at approximately 600 cm<sup>-1</sup> is also assigned to the second-order longitudinal acoustic (2LA) mode [47]. It is worth noting that the first-order Raman spectrum reflects the phonon density of states. The additional less intense Raman feature observed at 106 cm<sup>-1</sup> on the spectrum (d) in Figure 6 has been reported in Raman spectra of TiN coatings [46]. The other Raman features are assigned to the anatase and rutile phases of TiO<sub>2</sub>. The most intense band of anatase is identified at 150 cm<sup>-1</sup> whereas the two most intense bands of rutile are found at 440 and 600 cm<sup>-1</sup>. The band at 440 cm<sup>-1</sup> overlaps a TiN Raman band of low intensity. The most intense Raman feature of MoO<sub>2</sub> is also identified on the spectra. The bands of low intensity ranging at higher wave numbers are a convolution between MoO<sub>3</sub> Raman features and second-order Raman bands of TiN.

It is worth noting that the presence of oxides in amorphous or crystallized state is unavoidable in Mo–Ti/Si and Ti–Mo/Si bilayer films especially because Ti strongly reacts with the remaining oxygen.

In what follows, SIMS depth profiling measurements are carried out to evidence the diffusion of nitrogen into MoTi1 and TiMo3 bilayer films processed at 400 and 600 °C. The diffusion of Si, Ti and Mo through the bilayer films is also investigated.

### 3.2.2. Diffusion of Elements

#### SIMS Measurements

A total of 30 min of plasma exposure on MoTi1 heated at 400 °C results in the transfer of nitrogen into the Mo film compared with the corresponding as-received bilayer film in Figure 3. The nitrogen diffusion profile is indicated with the arrow on Figure 7. The other signals remain unchanged.

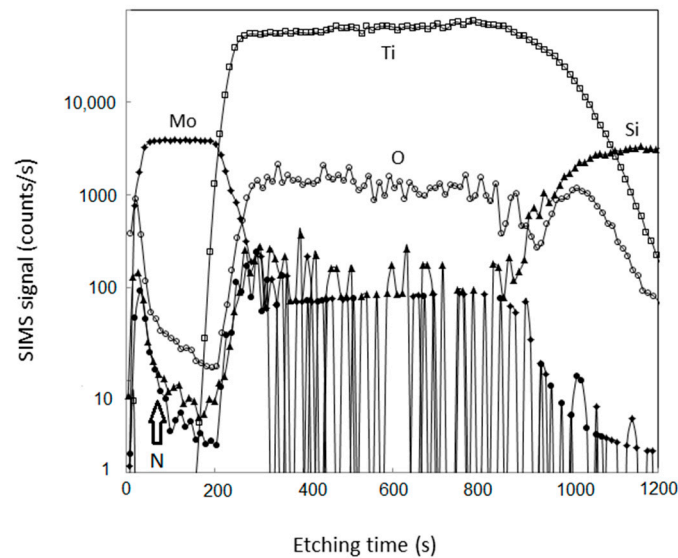


**Figure 7.** SIMS depth profile of MoTi1 bilayer film heated at 400 °C and processed in (Ar-31%N<sub>2</sub>-6%H<sub>2</sub>) plasma for 30 min.

Longer treatment duration promotes the diffusion of nitrogen into MoTi1. Nitrogen continues diffusing into the Mo film and then through the Mo–Ti interface into the Ti film (Figure 8).

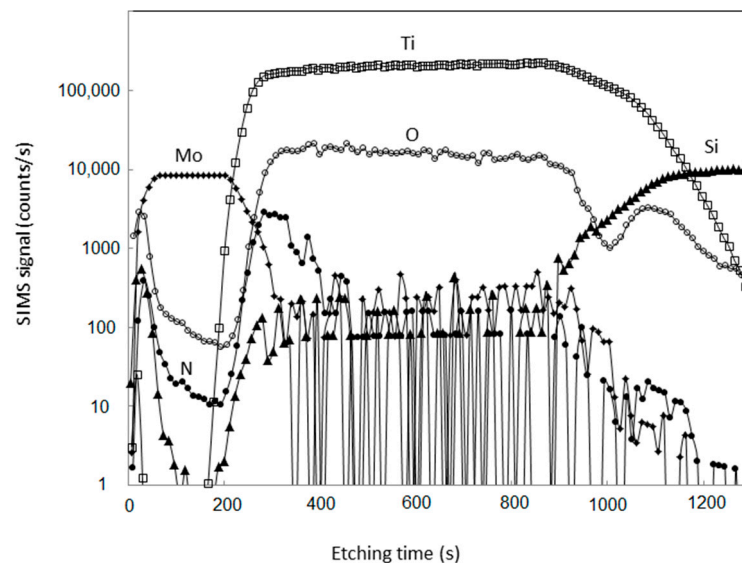


**Figure 8.** SIMS depth profile of MoTi1 bilayer film heated at 400 °C and processed in (Ar-31%N<sub>2</sub>-6%H<sub>2</sub>) plasma for 90 min.

An increase in substrate temperature from 400 °C to 600 °C results in a substantial modification in the form of all interfaces, which become broad (Figure 9).

The Ti–Si interface is reached after a much longer etching time, so the diffusion of Ti and Si through the Ti–Si interface continues in opposite directions. Si crosses the Ti film first and then the Mo film towards the surface. Its amount is roughly constant through both metal films. This result agrees with the formation of TiSi<sub>2</sub> and MoSi<sub>2</sub>, which have been previously reported by XRD and Raman spectroscopy measurements. The thickness of the Mo–Ti/Si bilayer film is more than twice as large as the thickness of the initial one, assuming a constant sputtering time. A similar result has been obtained in pure Ti films [1,27]. It is noticed that the diffusion of Si from the substrate up to the MoTi1 surface

goes with a strong depletion of the oxygen signal in the Ti film and a peak at the Ti–Mo interface. The diffusion of silicon towards the surface seems to push away oxygen which piles up at the Mo–Ti interface probably because Si and O elements occupy the same sites in Ti. Nitrogen seems also to be piled up at the same location. The segregation of N and O can induce breaks at the Mo–Ti interface. Such breaks have been observed in some MoTi1 bilayer films. It is worth noting that the diffusion of Si through MoTi1 and the formation of MoSi<sub>2</sub> prevent the crystallization of Mo nitrides. It is consistent with thermodynamic rules since the formation of MoSi<sub>2</sub> is greatly promoted compared with the formation of Mo<sub>2</sub>N, their enthalpies of formation are  $-137$  and  $-40.15$  kJ·mol<sup>-1</sup> at 300 K, respectively [48,49].

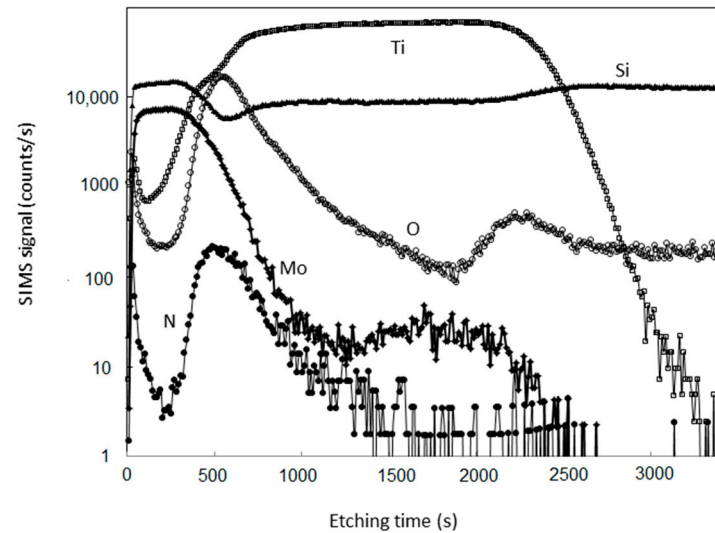


**Figure 9.** SIMS depth profile of MoTi1 bilayer film heated at 600 °C and processed in (Ar-31%N<sub>2</sub>-6%H<sub>2</sub>) plasma for 90 min.

The process of diffusion of Si, N and O and reaction with Ti and Mo seems over after plasma exposure at 600 °C for 1 h 30 min since a longer plasma exposure duration at 600 °C or similar plasma exposure durations at 800 °C only result in trifling changes.

In contrast with Figure 8, which displays a nitrogen diffusion profile through the Mo film in MoTi1, a large amount of nitrogen is incorporated in the Ti film located at the surface of TiMo3 processed at 400 °C for 30 min (Figure 10).

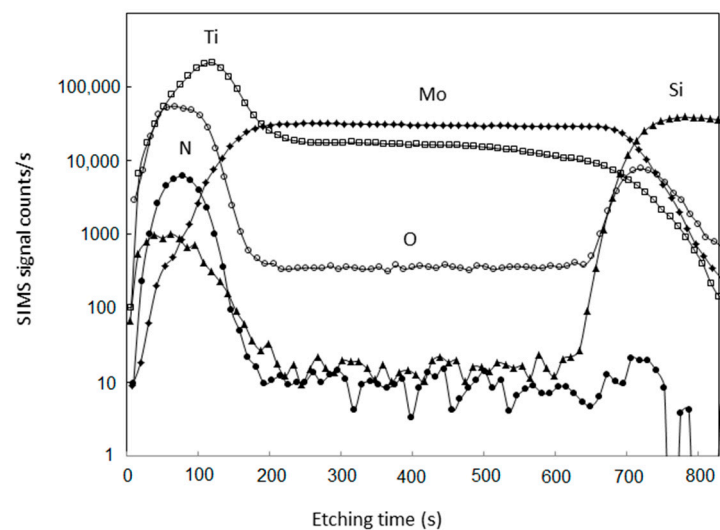


**Figure 10.** SIMS depth profile of TiMo3 bilayer film heated at 400 °C and processed in (Ar-31%N<sub>2</sub>-6%H<sub>2</sub>) plasma for 30 min.

Since the oxygen amount in the Ti film is high, the formation of Ti oxynitrides cannot be ruled out. The other SIMS signals remain unchanged. Nitrogen continues diffusing into the inner layers of TiMo<sub>3</sub> with increasing substrate temperature (Figure 11).

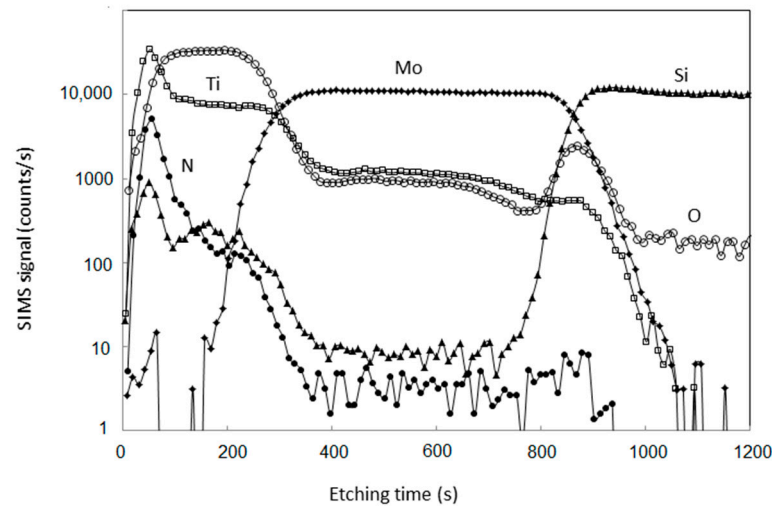


**Figure 11.** SIMS depth profile of TiMo<sub>3</sub> bilayer film heated at 600 °C and processed in (Ar-31%N<sub>2</sub>-6%H<sub>2</sub>) plasma for 30 min.

A nitrogen diffusion profile crossing the Ti film and the surface layers of the Mo film is clearly displayed. However, in contrast with MoTi1, the Mo–Si interface is still well identified. The Mo film forms a barrier of diffusion preventing Si from diffusing towards the surface at temperatures of 600 °C and lower. However, a quite puzzling effect occurred in the surface layers of TiMo<sub>3</sub>. The Mo SIMS signal seems to have shifted towards the inner layers compared with the Mo signal displayed in Figures 4 and 10 and thus, the surface layers of TiMo<sub>3</sub> only consist of Ti instead of a solid solution of Ti and Mo. A slight change in slope of the nitrogen SIMS signal is also seen in the vicinity of the new Ti–Mo interface which is related to the occurrence of a second diffusion mode of nitrogen. Such an effect can be correlated to the crystallization of TiN in the surface layers of TiMo<sub>3</sub>. The apparent shift of the Mo signal is due to the formation and growth of TiN crystallites which form an additional film at the surface drawing back Mo. This effect goes with the lowering of the etching rate in the TiN crystallized film during SIMS experiments.

#### EDS Measurements

The huge increase in the whole thickness of the MoTi1 bilayer film after the plasma treatment as well as the conspicuous behavior of oxygen at Mo–Ti interface are well confirmed in Figure 12 which displays the concentration of Ti, Mo, Si and O (at%) along a line scan carried out across the MoTi1 bilayer film processed in plasma at 600 °C for 3 h.

The thickness of Mo and Ti layers is twice the thickness of Mo and Ti films in MoTi1 bilayer film before the plasma treatment, respectively, and the peak of O at Ti–Mo interface is due to the Si diffusion which pushed O away from Ti layer up to the Mo–Ti interface where it is trapped.

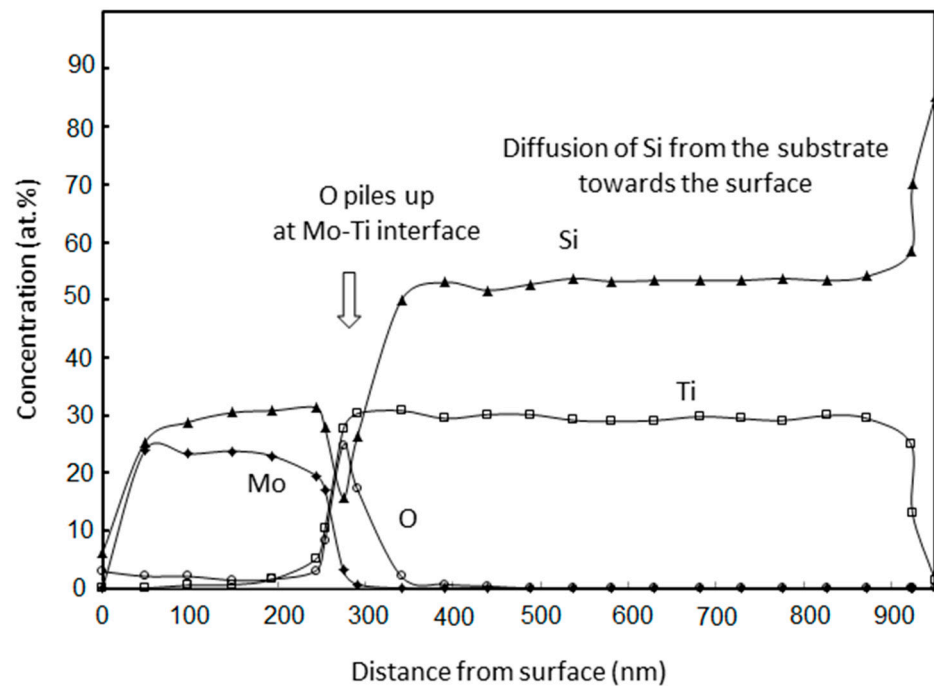


**Figure 12.** EDS line scan results providing the concentration of Mo, Ti, Si and O (at.%) in MoTi1 heated at 600 °C and processed in (Ar-31%N<sub>2</sub>-6%H<sub>2</sub>) plasma for 3 h.

### 3.2.3. Morphology and Microstructures of MoTi1 Bilayer Thin Films

Since TiMo1, TiMo2 and TiMo3 consist of TiN crystallites according to XRD and Raman measurements, the surface is formed with faceted grains of nanometric size with triangular geometry. This is consistent with previous works on Ti-Mo/Si bilayer films of larger thicknesses [29]. Therefore, in what follows, only MoTi1 is investigated.

The morphology of MoTi1 heated at 600 °C and exposed to (Ar-31%N<sub>2</sub>-6%H<sub>2</sub>) plasma for 3 h and investigated by SEM is displayed in Figure 13.

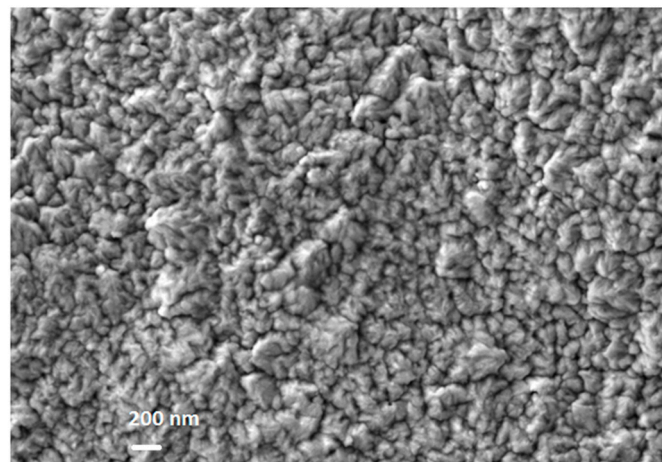


**Figure 13.** SEM image of the surface of MoTi1 heated at 600 °C and processed in (Ar-31%N<sub>2</sub>-6%H<sub>2</sub>) plasma for 3 h.

The surface of MoTi1 is slightly rough and displays grains of nanometric size, which consist of tiny crystallites embedded in a smooth and amorphous-like gangue. In spite of these structures, the surface shows a continuous coverage. It is worth noting that these structures tend to form tips oriented towards the direction of growth perpendicular to the surface.

Cross-sectional TEM and SAED measurements are also carried out. As seen on the electron micrographs (a) and (b) in Figure 14, the MoTi1 bilayer film mainly consists of two distinct crystallized layers which appear rather rough and are formed of round-shaped nanostructures and square shaped crystallites of nanometric size.

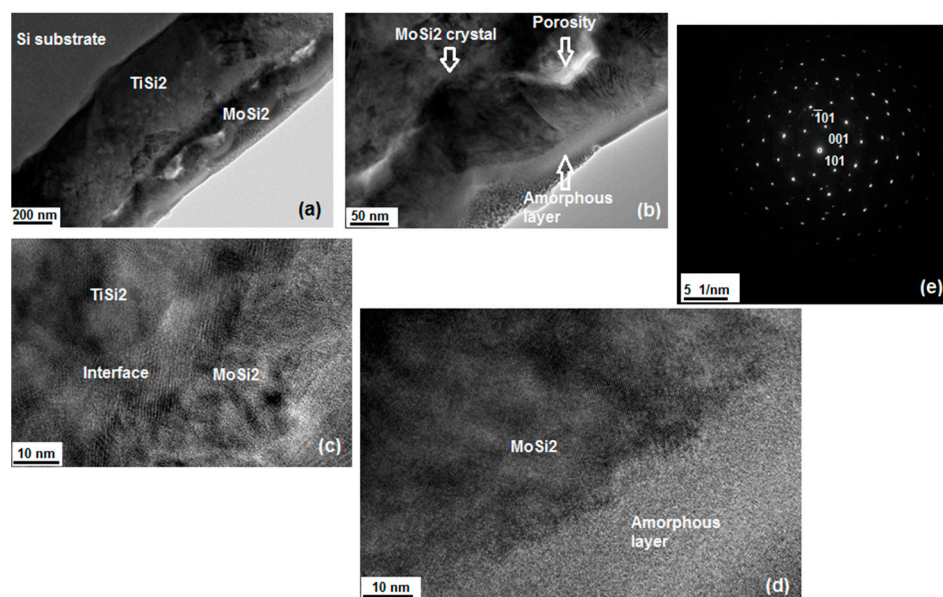


**Figure 14.** Electron micrographs of MoTi1 heated at 600 °C and processed in (Ar-31%N<sub>2</sub>-6%H<sub>2</sub>) plasma for 3 h (a) and (b) HRTEM electron micrographs of TiSi<sub>2</sub>-MoSi<sub>2</sub> interface (c) and MoSi<sub>2</sub>-amorphous layer interface (d) SAED pattern of MoSi<sub>2</sub> crystallites (e).

Because of the strong intermixing of Si, Ti and Mo at Ti-Si and Mo-Ti interfaces, both layers strongly grow to reach a thickness of twice that measured before the plasma treatment is approximately twice the thickness of the as-deposited bilayer film. The value of the whole thickness of MoTi1 ranges between 710 and 750 nm. The figures display that both Ti-Si and Mo-Ti interfaces are slightly wavy-like. A third layer, thinner than the former, is also seen next to the surface of MoTi1. It is rather amorphous. The layer adjacent to the Si substrate exhibits a columnar structure in the direction of growth and consists of round-shaped crystallites of large sizes. Such structures have already been identified in pure Ti films coated on Si substrates and processed under similar experimental conditions. They have been assigned to TiSi<sub>2</sub> crystallites [28]. The bubble-like inclusions displayed in the crystallites have been reported to belong to the crystal lattice and not to gas inclusions as it was reported in former works. The layer adjacent to the amorphous layer mainly consists of square-shaped crystallites of various sizes. A crystal of larger dimension of approximately 110 × 150 nm<sup>2</sup> is displayed in the electron micrograph (b) Figure 14. It crosses the Mo film up to the amorphous layer. This crystal is expected to be MoSi<sub>2</sub>. The structures of bright colors are porosities which formed close to the Mo-Ti interface. They can be due to the segregation of oxygen and nitrogen at the Mo-Ti interface identified by SIMS and EDS measurements. The presence of such porosities makes the interface breakable. This result explains the fact that some MoTi1 bilayer films have been damaged.

In addition to the porosities, the interface between both crystallized layers is continuous and the crystallites of TiSi<sub>2</sub> and MoSi<sub>2</sub> seem closely entangled (Figure 14c). Moreover, the surroundings of the porosities seem covered with very tiny crystallites. Since the color of these crystallites is lighter than that of the crystals of TiSi<sub>2</sub> and MoSi<sub>2</sub>, they could be mainly consist of Si since the electron beam is less absorbs by lighter element. This phenomenon could be explained by the fact that Si diffuses from the substrate through the TiSi<sub>2</sub> layer and reacts with Mo to form MoSi<sub>2</sub>. The excess of Si crystallizes at the Mo-Ti interface, making it breakable.

The interface between MoSi<sub>2</sub> and the amorphous layer is continuous (Figure 14d) and the morphology confirms the result obtained by SEM measurements (see Figure 13) since tips oriented towards the direction of growth are displayed. On the other hand, the amorphous layer could consist of Mo nitrides since SIMS measurements performed on MoTi1 processed at 400 °C and 600 °C display the diffusion of nitrogen into the surface layers of the Mo–Ti/Si bilayer film.

The SAED pattern (e) in Figure 14 has been taken on the crystal of larger dimensions (see Figure 14b). It confirms that the film adjacent to the amorphous layer mainly consists of MoSi<sub>2</sub> crystallites. This crystal is identified as the β phase of MoSi<sub>2</sub> of hexagonal structure. The crystal is oriented along its [101] axis.

### 3.3. Mo–Ti/Si and Ti–Mo/Si Bilayer Films Exposed to (Ar-31%N<sub>2</sub>-6%H<sub>2</sub>) at 800 °C

#### 3.3.1. Crystalline Structures

##### XRD Investigations

Compared with MoTi1 processed at 600 °C, the XRD pattern corresponding to MoTi1 heated at 800 °C and exposed to (Ar-31%N<sub>2</sub>-6%H<sub>2</sub>) plasma for 1 h 30 min, no clear changes are displayed on the XRD pattern (a) Figure 15. However, an additional very thin diffraction line at 2θ of approximately 28.45° is displayed on the pattern and can be assigned to the most intense reflection of the (111) atomic planes of polycrystalline Si (JCPDS card n° 04-001-7247). Two other very tiny peaks, at 2θ of approximately 47.32° and 56.14° corresponding to the (220) and (311) reflection lines, are also identified on the pattern. Such an appearance of polycrystalline Si in thin metal films coated on Si substrates has already been reported during the growth of TiN at the expense of TiSi<sub>2</sub> in pure Ti films processed under similar experimental conditions. Such an effect has been assigned to the release of Si during the reaction between TiSi<sub>2</sub> and nitrogen to produce TiN [28].

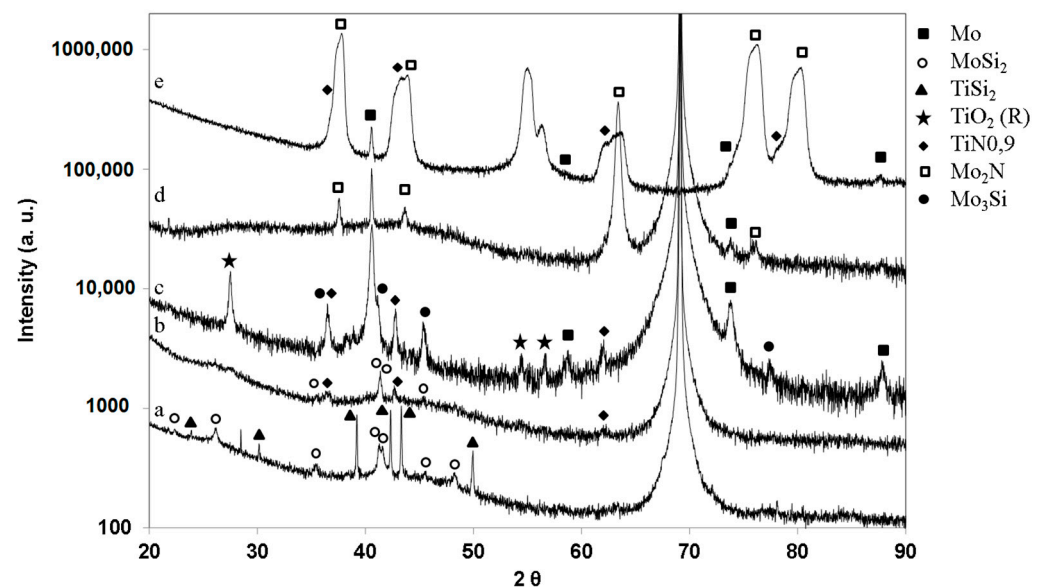


**Figure 15.** Conventional X-ray diffraction patterns of Mo–Ti bilayer films heated at 800 °C and processed in (Ar-31%N<sub>2</sub>-6%H<sub>2</sub>) plasma for 90 min, MoTi1 (a), TiMo1 (b), TiMo2 (c) and TiMo3 (d). Grazing angle X-ray diffraction of TiMo3 bilayer film heated at 800 °C and processed in (Ar-31%N<sub>2</sub>-6%H<sub>2</sub>) plasma for 3 h (e).

With regard to TiMo1, TiMo2 and TiMo3 bilayer films processed under the same experimental conditions, the increase in the substrate temperature up to 800 °C results in the growth of TiN phase. All XRD patterns except (d) Figure 15, because of the small thickness of the Ti film at the surface of TiMo3, display the most intense (111) and (200) reflection lines of TiN. It coexists with the rutile phase of TiO<sub>2</sub> in TiMo1 with very tiny

peaks (Figure 15 (b)) and TiMo2 (Figure 15 (c)). Pure Mo remains in all MoTi bilayer films except in TiMo1 where Mo turns into  $\beta$ MoSi<sub>2</sub> of hexagonal structure (Figure 15 (b)). The XRD pattern (c) corresponding to TiMo2 displays two reflection lines at  $2\theta$  of approximately  $45.45^\circ$  and  $78^\circ$  which corresponds to the (211) and (400) reflection lines of the Mo<sub>3</sub>Si phase of cubic structure (JCPDS card n° 04-004-2955). The (200) and (210) diffraction peaks are overlapped by TiN and pure Mo ones at Bragg angles of approximately  $36.45^\circ$  and  $41.18^\circ$ , respectively. As previously seen for TiMo3 processed at  $600^\circ\text{C}$ , because of the low thickness of the Ti film, TiN cannot be identified with conventional XRD measurements. However, well-crystallized  $\gamma$ Mo<sub>2</sub>N of cubic structure (JCPDS card n° 00-025-1366) is clearly displayed since the (111), (200), (220), (311) and (222) diffraction lines are identified (Figure 15 (d)). The Mo<sub>2</sub>N phase exhibits a very strong (220) preferred orientation as in pure Mo film processed under the same experimental conditions [30]. Since these diffraction lines are slightly shifted towards higher Bragg angles, Mo<sub>2</sub>N would be slightly under stoichiometric.

Grazing angle XRD measurements have been carried out on TiMo3 processed for 3 h. The corresponding XRD pattern shows that  $\gamma$ Mo<sub>2</sub>N crystallites coexist with TiN crystallites (Figure 15 (e)). The reflection at a Bragg angle of approximately  $41.5^\circ$  corresponding to pure Mo remains. However, no Ti oxides is identified, they all turned into TiN at the surface of the TiMo3 bilayer film. The peak at a Bragg angle of approximately  $55^\circ$  is unidentified but it likely corresponds to impurities which remain at the surface of the bilayer films.

#### Raman Spectroscopy Investigations

No huge changes are identified after processing the MoTi1 bilayer film at  $800^\circ\text{C}$ . The Raman spectrum corresponding to the MoTi1 bilayer film heated at  $800^\circ\text{C}$  and exposed to (Ar-31%N<sub>2</sub>-6%H<sub>2</sub>) plasma for 1 h 30 min (Figure 16 (a)) is almost the same as that obtained at a substrate temperature of  $600^\circ\text{C}$ .

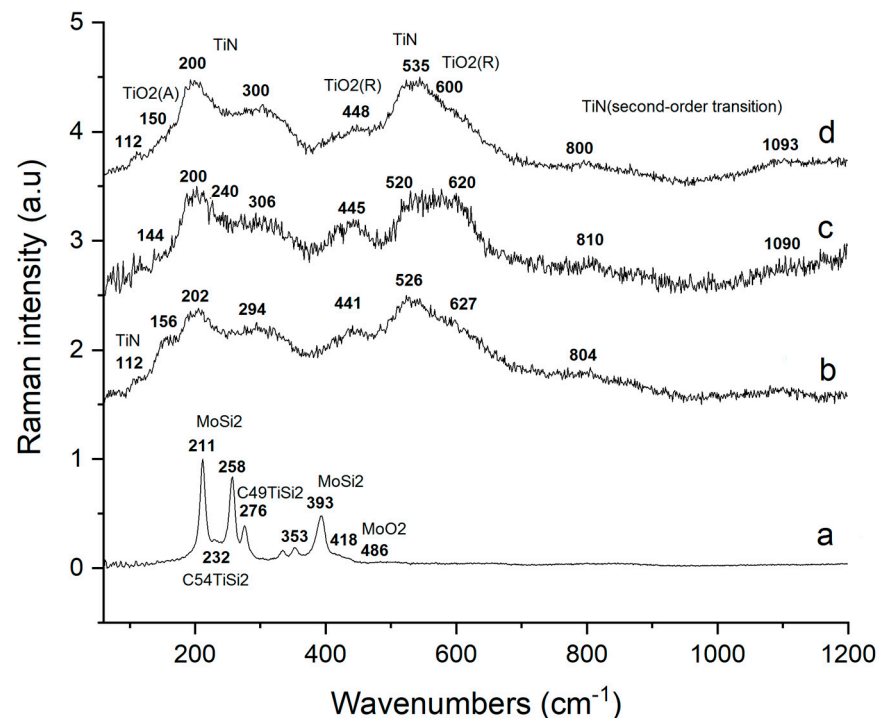


**Figure 16.** Raman scattering spectra of Mo-Ti bilayer films. MoTi1 heated at  $800^\circ\text{C}$  and processed in (Ar-31%N<sub>2</sub>-6%H<sub>2</sub>) plasma for 90 min (a), TiMo1, TiMo2, and TiMo3 heated at  $800^\circ\text{C}$  and processed in (Ar-31%N<sub>2</sub>-6%H<sub>2</sub>) plasma for 90 min (b), 30 min (c) and 90 min (d), respectively.

However, a decrease in the intensity of the broad Raman features corresponding to titanium and molybdenum oxides is also observed. The reduction of metal oxides by the plasma species is more efficient at  $800^\circ\text{C}$ .

In contrast with MoTi1, the structures of the Raman spectra corresponding to TiMo1, TiMo2 and TiMo3 are drastically modified because of the growth and crystallization of the TiN phase at high temperatures (Figure 16 (b), (c) and (d)) This is especially identified with the strong increase in the intensity of the Raman signal in the optical frequency range at 500–600  $\text{cm}^{-1}$  and with the increase in the intensity of the second-order acoustic and optical modes in the wave number range from 800 to 1200  $\text{cm}^{-1}$ . In the same way as we have seen for MoTi1, a reduction of Mo and Ti oxides is also identified.

#### 4. Discussion

Some mechanisms of formation of nitrides and silicides in Mo–Ti and Ti–Mo bilayer films coated on Si substrates, which differ from each other by various thicknesses and locations of Mo and Ti films relative to Si substrates, have been evidenced after processing in expanding ( $\text{Ar-31\%N}_2\text{-6\%H}_2$ ) plasma at various temperatures and treatment durations. The diffusion of Ti, Si and Mo through Mo–Ti/Si and Ti–Mo/Si bilayer films as well as the diffusion of nitrogen into the surface layers result in the formation and crystallization of nitrides and silicides which are thermodynamically and kinetically controlled. These compounds are well known to exhibit interesting properties for a wide range of applications.

Ti metal is very reactive towards Si so, strong Ti–Si intermixing occurs at the Ti–Si interface in the MoTi bilayer film which consists of Ti film adjacent to the Si substrate. The formation of a disorder region with a composition close to TiSi or the formation of amorphous Ti–Si alloys at temperatures ranging between 300 and 400 °C have been widely reported in former works [2,27,37,41]. In the present work, the process described above starts during the evaporation of Ti films on Si wafers and continues during the plasma treatment at 400 °C. The diffusion of nitrogen into the Mo film located at the surface and beyond the Mo–Ti interface occurs simultaneously and in the opposite direction. Nitrogen results from the reaction of  $\text{NH}_x$  species produced in the plasma with the solid surface. At a substrate temperature of 600 °C, Si widely diffuses throughout the Mo–Ti/Si bilayer film up to the surface. It successively results in the formation and crystallization of TiSi<sub>2</sub> and MoSi<sub>2</sub> which prevent the crystallization of Mo nitrides at surface. TiSi<sub>2</sub> displays round-shaped crystallites whereas MoSi<sub>2</sub> rather exhibits square-shaped crystallites of nanometric size.

On its way from the substrate to the surface, Si pushes away oxygen from the Ti film as well as nitrogen, which pile up at the Mo–Ti interface and make Mo–Ti/Si bilayer films breakable. This process is consistent with thermodynamic data available for metal nitrides and silicides, since the enthalpy of formation of MoSi<sub>2</sub> and TiSi<sub>2</sub> are far below that of Mo<sub>2</sub>N which are  $-137$ ,  $-134$  and  $-40.15$   $\text{kJ}\cdot\text{mol}^{-1}$  at 300 K, respectively [48–50]. In contrast, the crystallization of Mo silicides does not occur in pure Mo films coated on Si substrates and heated at 600 °C, which makes the crystallization of Mo nitrides possible [30]. The crystallization of MoSi<sub>2</sub> is promoted at the TiSi<sub>2</sub>–Mo interface. It is worth noting that the growth of TiSi<sub>2</sub> is reported to be diffusion controlled [7] whereas the formation of MoSi<sub>2</sub> is nucleation controlled [51]. The increase in substrate temperature up to 800 °C mainly results in the growth of the MoSi<sub>2</sub> phase and the crystallization of the excess of diffusing Si which forms polycrystals.

Regarding Ti–Mo/Si bilayer films, the Mo film adjacent to the Si wafer, a large amount of nitrogen is stored in the Ti film at a substrate temperature of 400 °C. Nitrogen diffuses beyond the Ti–Mo interface into the Mo film at 600 °C. On the other hand, a new interface is identified with the formation of TiN crystallites at the surface of the Mo–Ti bilayer film.

In contrast with Mo–Ti/Si bilayer films, the Ti film adjacent to the Si wafer, Si does not diffuse from the substrate heated at 600 °C. A Mo film, only 50 nm thick, and coated on Si wafer prevents the diffusion of Si and then the formation and crystallization of Mo and Ti silicides. Owing to the Mo barrier of diffusion, the crystallization of TiN is promoted and TiN coexists with the remaining TiO<sub>2</sub> phase. Because of the strong affinity of Ti towards oxygen, TiN is mainly the result of the reaction of TiO<sub>2</sub> with nitrogen, which is mainly provided by  $\text{NH}_x$  radicals produced in the plasma. The reactivity of the surface is improved by the impinging  $\text{NH}_x$  radicals and/or H atoms by means of their

reducing effects on remaining oxides. According to thermodynamic data, the enthalpy of formation of  $\text{TiO}_2$  is far below that corresponding to  $\text{TiN}$ . They are  $-944 \text{ kJ}\cdot\text{mol}^{-1}$  [38] and  $-337.45 \text{ kJ}\cdot\text{mol}^{-1}$  [50] at 500 K, respectively. In spite of the large difference between these values, the formation of  $\text{TiN}$  from  $\text{TiO}_2$  and nitrogen is possible. This is the result of the occurrence of exothermic reactions which involve the formation of intermediates and/or  $\text{H}_2\text{O}$  and promote the formation of  $\text{TiN}$ . Such an effect has been evidenced in the formation of  $\gamma\text{Mo}_2\text{N}$  of cubic structure during a reduction–nitridation process reported in a former work [30].

At a substrate temperature of 800 °C, the Mo barrier of diffusion is no longer efficient since various Mo silicides crystallize depending on the thickness of Ti and Mo films. The Mo/Si ratio is correlated with the thickness of Ti and Mo films since the thicker the Mo film, the larger the Mo/Si ratio. However, owing to the lack of Mo silicides in the Mo film, 250 nm thick, adjacent to the Si substrate, Mo nitrides crystallize in the  $\gamma\text{Mo}_2\text{N}$  phase of cubic structure, which coexists with the  $\text{TiN}$  phase in the Ti–Mo/Si bilayer film.

## 5. Conclusions

The expanding plasma process using a microwave discharge of 2.45 GHz, which promotes chemical reactions on the surface of thin films, has been successfully employed to carry out nitriding treatments on Mo–Ti/Si and Ti–Mo/Si bilayer thin films of various thicknesses and locations with respect to Si wafers. Plasma species such as  $\text{NH}_x$  radicals and/or H atoms, play a great role in reducing oxides compounds during exothermic reactions which involve the formation of intermediates and/or  $\text{H}_2\text{O}$  and results in the improvement of the diffusion of nitrogen into the surface layers. A reduction–nitridation process has been evidenced during the nitriding plasma treatment of Mo films [30]. Because of the great reactivity of Ti, Si diffuses from the Si substrate through the Mo–Ti/Si bilayer film. It results in the crystallization of both  $\text{TiSi}_2$  and  $\text{MoSi}_2$  at a temperature of 600 °C and the segregation of oxygen and nitrogen at the Mo–Ti interface. In contrast, a Mo thin film, only 50 nm thick, adjacent to Si wafer is a good barrier of diffusion which prevents the transfer of Si through the Ti–Mo/Si bilayer films and the formation of silicides at 600 °C, allowing  $\text{TiN}$  to crystallize. However, this barrier is no longer efficient at higher temperatures, since, at a substrate temperature of 800 °C, Mo silicides crystallize and the thicker the Mo film, the larger the Mo/Si ratio. The lack of crystallized Mo silicides in the Ti–Mo/Si bilayer film which consists of a Mo film, 250 nm thick, allows the  $\text{Mo}_2\text{N}$  phase of cubic structure to crystallize and coexist with  $\text{TiN}$  crystallites. The role of plasma species in the reducing of oxide compounds, which remains in very reactive thin films of transition metals, continues to be investigated. Further studies including bilayer thin films, which consist of other transition metals such as vanadium, are planned.

**Author Contributions:** Conceptualization, I.J. and J.L.J.; methodology, I.J. and A.B.; validation, I.J., J.L.J. and A.B.; formal analysis, I.J.; investigation, R.M., J.C., P.C., D.M., A.B. and A.P.; data curation, I.J. and R.M.; writing—original draft preparation, I.J. All authors have read and agreed to the published version of the manuscript.

**Funding:** This research received no external funding.

**Acknowledgments:** Région Limousin is acknowledged for the support of work on the surface reactivity.

**Conflicts of Interest:** The authors declare no conflict of interest.

## References

1. Bhaskaran, M.; Sriram, S.; Short, K.T.; Mitchell, D.R.G.; Holland, A.S.; Reeves, G.K. Characterization of C54 titanium silicide thin films by spectroscopy, microscopy and diffraction. *J. Phys. D Appl. Phys.* **2007**, *40*, 5213–5219. [[CrossRef](#)]
2. Jeon, H.; Sukow, C.A.; Honeycutt, J.W.; Rozgonyi, G.A.; Nemanich, R.J. Morphology and phase stability of  $\text{TiSi}_2$  on Si. *J. Appl. Phys.* **1992**, *71*, 4269–4276. [[CrossRef](#)]
3. Yanisagawa, S.; Fukuyama, T. Preparation of molybdenum silicide films by reactive sputtering. *J. Electrochem. Soc.* **1980**, *127*, 1120–1124. [[CrossRef](#)]

4. Ke-Ming, Y.; Jun-Xia, W.; Shi-Yuan, Y.; Xiu-Lu, Z.; Ping, L. In-situ synthesis of MoSi<sub>2</sub> coating on Mo substrate under carbon protection and its short-term oxidation behavior. *Surf. Coat. Technol.* **2018**, *354*, 324–329. [[CrossRef](#)]
5. Ohishi, Y.; Kurosaki, K.; Suzuki, T.; Muta, H.; Yamanaka, S.; Uchida, N.; Tada, T.; Kanayama, T. Synthesis of silicon and molybdenum-silicide nanocrystal composite films having low thermal conductivity. *Thin Solid Films* **2013**, *534*, 238–241. [[CrossRef](#)]
6. Liu, Z.; Luo, B.; Hu, J.; Xing, C. Transport mechanism in amorphous molybdenum silicide thin films. *J. Phys. Chem. Solids* **2021**, *149*, 109818. [[CrossRef](#)]
7. Iyer, S.S.; Ting, C.Y.; Fryer, P.M. Ambient gas effects on the reaction of titanium with silicon. *J. Electrochem. Soc.* **1985**, *132*, 2240–2245. [[CrossRef](#)]
8. Tsai, J.Y.; Apte, P. A thickness model for the TiSi<sub>2</sub>/TiN stack in the titanium silicide process module. *Thin Solid Films* **1995**, *270*, 589–595. [[CrossRef](#)]
9. Lee, W.G.; Lee, J.G. Enhancement of TiSi<sub>2</sub> formation during rapid thermal annealing in N<sub>2</sub> by the presence of native oxide. *J. Electrochem. Soc.* **2002**, *149*, G1–G7. [[CrossRef](#)]
10. Wang, L.L.; Peng, W.; Jiang, Y.L.; Li, B.Z. Effective Schottky barrier height lowering by TiN capping layer for TiSi<sub>x</sub>/Si power diode. *IEEE Electron Device Lett.* **2015**, *36*, 597–599. [[CrossRef](#)]
11. Oyama, S.T. Introduction to the chemistry of transition metal carbides and nitrides. In *The Chemistry of Transition Carbides and Nitrides*, 1st ed.; Oyama, S.T., Ed.; Blackie Academic and Professional: London, UK, 1996; pp. 2–10.
12. Jauberteau, I.; Bessaudou, A.; Mayet, R.; Cornette, J.; Jauberteau, J.L.; Carles, P.; Merle-Méjean, T. Molybdenum nitride films: Crystal structures, synthesis, mechanical, electrical and some other properties. *Coatings* **2015**, *5*, 656–687. [[CrossRef](#)]
13. Ozsdolay, B.D.; Balasubramanian, K.; Gall, D. Cation and anion vacancies in cubic molybdenum nitride. *J. All. Com.* **2017**, *705*, 631–637. [[CrossRef](#)]
14. Ponon, N.K.; Appleby, D.J.R.; Arac, E.; King, P.J.; Ganti, S.; Kwa, K.S.K.; O'Neill, A. Effect of deposition conditions and postdeposition anneal on reactively sputtered titanium nitride films. *Thin Solid Films* **2015**, *578*, 31–37. [[CrossRef](#)]
15. Lima, L.P.B.; Diniz, J.A.; Doi, I.; Godoy Fo, J. Titanium nitride as electrode for MOS technology and Schottky diode: Alternative extraction method of titanium nitride work function. *Microelectron. Eng.* **2012**, *92*, 86–90. [[CrossRef](#)]
16. Xiang, W.; Zhao, C.; Liu, K.; Zhang, G.; Zhao, K. Heteroepitaxial growth of TiN thin films on Si substrates for MEMS applications. *J. Alloys Compd.* **2016**, *658*, 862–866. [[CrossRef](#)]
17. Tagliuzucca, V.; Schlichte, K.; Schüth, F.; Weidenthaler, C. Molybdenum-based catalysts for the decomposition of ammonia: In situ X-ray diffraction studies, microstructure, and catalytic properties. *J. Catal.* **2013**, *305*, 277–289. [[CrossRef](#)]
18. Tagliuzucca, V.; Leoni, M.; Weidenthaler, C. Crystal structure and microstructural changes of molybdenum nitrides traces during catalytic reaction by in situ X-ray diffraction studies. *Phys. Chem. Chem. Phys.* **2014**, *16*, 6182–6188. [[CrossRef](#)]
19. Zhu, J.F.; Guo, J.C.; Zhai, R.S.; Bao, X.; Zhang, X.Y.; Zhuang, S. Preparation and adsorption properties of Mo<sub>2</sub>N model catalyst. *Appl. Surf. Sci.* **2000**, *161*, 86–93. [[CrossRef](#)]
20. Zhou, Y.; Guo, W.; Li, T. A review on transition metal nitrides as electrode materials for supercapacitors. *Ceram. Int.* **2019**, *45*, 21062–21076. [[CrossRef](#)]
21. Xiong, Z.; Yang, J.; Gao, Z.; Yang, Q.; Shi, D. Orthorhombic Mo<sub>3</sub>N<sub>2</sub> nanobelts with improved properties as electrode material for supercapacitors. *Results Phys.* **2020**, *16*, 102941. [[CrossRef](#)]
22. Bernie Ting, Y.-J.; Wu, H.; Kherani, N.P.; Lian, K. Development of pseudocapacitive molybdenum oxide-nitride for electrochemical capacitors. *Mater. Chem. Phys.* **2015**, *154*, 118–124. [[CrossRef](#)]
23. Gu, M.; Bai, S.; Xia, X.; Huang, X.; Li, X.; Shi, X.; Chen, L. Study of the high temperature interfacial stability of Ti/Mo/Yb<sub>0.3</sub>Co<sub>4</sub>Sb<sub>12</sub> thermoelectric joints. *Appl. Sci.* **2017**, *7*, 952. [[CrossRef](#)]
24. Bernie Ting, Y.-J.; Lian, K.; Kherani, N. Fabrication of titanium nitride and molybdenum nitride for supercapacitor electrode application. *ECS Trans.* **2011**, *35*, 133–139. [[CrossRef](#)]
25. Xie, Y.; Tian, F. Capacitive performance of molybdenum nitride/titanium nitride nanotube array for supercapacitor. *Mater. Sci. Eng. B* **2017**, *215*, 64–70. [[CrossRef](#)]
26. Klimashin, F.F.; Koutna, N.; Euchner, H.; Holec, D.; Mayrhofer, P.H. The impact of nitrogen content and vacancies on structure and mechanical properties of Mo-N thin films. *J. Appl. Phys.* **2016**, *120*, 185301. [[CrossRef](#)]
27. Jauberteau, I.; Mayet, R.; Cornette, J.; Mangin, D.; Bessaudou, A.; Carles, P.; Jauberteau, J.L.; Passelergue, A. Silicides and nitrides formation in Ti films coated on Si and exposed to (Ar-N<sub>2</sub>-H<sub>2</sub>) expanding plasma. *Coatings* **2017**, *7*, 23. [[CrossRef](#)]
28. Jauberteau, I.; Carles, P.; Mayet, R.; Cornette, J.; Bessaudou, A.; Jauberteau, J.L. Competing growth of titanium nitrides and silicides in Ti films processed in expanding microwave plasma: Morphology and microstructural properties. *AIP Adv.* **2018**, *8*, 095105. [[CrossRef](#)]
29. Jauberteau, I.; Mayet, R.; Cornette, J.; Carles, P.; Mangin, D.; Bessaudou, A.; Jauberteau, J.L.; Passelergue, A. Expanding plasma process for nitriding Mo-Ti bilayer thin films. *Coatings* **2019**, *9*, 96. [[CrossRef](#)]
30. Jauberteau, I.; Mayet, R.; Cornette, J.; Bessaudou, A.; Carles, P.; Jauberteau, J.L.; Merle-Méjean, T. A reduction-nitridation process of molybdenum films in expanding microwave plasma: Crystal structure of molybdenum nitrides. *Surf. Coat. Technol.* **2015**, *270*, 77–85. [[CrossRef](#)]
31. Zaumseil, P. High resolution characterization of the forbidden Si(200) and Si(222) reflections. *J. Appl. Cryst.* **2015**, *48*, 528–532. [[CrossRef](#)]

32. Wang, J.; Coppari, F.; Smith, R.F.; Eggert, J.H.; Lazicki, A.E.; Fratanduono, D.E.; Rygg, J.R.; Boelhy, T.R.; Collins, G.W.; Duffy, T.S. X-ray diffraction of molybdenum under shock compression to 450 GPa. *Phys. Rev. B* **2015**, *62*, 174114. [[CrossRef](#)]
33. Oliveira, N.T.C.; Aleixo, G.; Caram, R.; Guastaldi, A.C. Development of Ti-Mo alloys for biomedical applications: Microstructures and electrochemical characterization. *Mater. Sci. Eng. A* **2007**, *452–453*, 727–731. [[CrossRef](#)]
34. Simka, W.; Krzakala, A.; Korotin, D.M.; Zhidkov, I.S.; Kurmaev, E.Z.; Cholakh, S.O.; Kuna, K.; Dercz, G.; Michalska, J.; Suchanek, K.; et al. Modification of a Ti-Mo alloy surface via plasma electrolytic oxidation in a solution containing calcium and phosphorus. *Electrochem. Acta* **2013**, *96*, 180–190. [[CrossRef](#)]
35. Zhang, W.-D.; Liu, Y.; Wu, H.; Song, M.; Zhang, X.-D.; Lan, X.-D.; Yao, T.-H. Elastic modulus of phases in Ti-Mo alloys. *Mater. Charact.* **2015**, *106*, 302–309. [[CrossRef](#)]
36. Kislitin, S.B.; Potekaev, A.I.; Uglov, V.V.; Klopotov, A.A.; Klopotov, V.D.; Ivanov, Y.F.; Parpiev, A.T. Steel surface TiCrN, TiMoN coatings structural phase state change features after low-energy alpha particles irradiation. *IOP Conf. Ser. Mater. Sci. Eng.* **2018**, *289*, 012010. [[CrossRef](#)]
37. Nemanich, R.J.; Fiordalice, R.W.; Jeon, H. Raman scattering characterization of titanium silicide formation. *IEEE J. Quantum Electron.* **1989**, *25*, 997–1002. [[CrossRef](#)]
38. Barhai, P.K.; Kumari, N.; Banerjee, I.; Pabi, S.K.; Mahapatra, S.K. Study of the effect of plasma current density on the formation of titanium nitride and titanium oxynitride thin films prepared by reactive DC magnetron sputtering. *Vacuum* **2010**, *84*, 896–901. [[CrossRef](#)]
39. Birtill, J.J.; Dickens, P.G. Thermochemistry of hydrogen molybdenum bronze phases  $H_xMoO_3$ . *J. Solid State Chem.* **1979**, *29*, 367–372. [[CrossRef](#)]
40. Zhang, S.-L.; Lavoie, C.; Cabral, C.; Harper, J.M.E.; d’Heurle, F.M.; Jordan-Sweet, J. In situ characterization of titanium silicide formation: The effect of Mo interlayer, temperature ramp-rate, and annealing atmosphere. *J. Appl. Phys.* **1999**, *85*, 2617–2626. [[CrossRef](#)]
41. Chaix-Pluchery, O.; Chenevier, B.; Matko, I.; Senateur, J.P.; La Via, F. Investigations of transient phase formation in Ti/Si thin film reaction. *J. Appl. Phys.* **2004**, *96*, 361–368. [[CrossRef](#)]
42. Doland, C.M.; Nemanich, R.J. Phase formation during reactive molybdenum-silicide formation. *J. Mater. Res.* **1990**, *5*, 2854–2864. [[CrossRef](#)]
43. Wdowik, U.D.; Twardowska, A.; Medala-Wasik, M. Lattice dynamics of binary and ternary phases in Ti-Si-C system: A combined Raman spectroscopy and density functional theory study. *Mater. Chem. Phys.* **2015**, *168*, 58–65. [[CrossRef](#)]
44. Dieterle, M.; Mestl, G. Raman spectroscopy of molybdenum oxides. *Phys. Chem. Chem. Phys.* **2002**, *4*, 812–826. [[CrossRef](#)]
45. Teoh, L.G.; Lee, Y.C.; Chang, Y.S.; Fang, T.H.; Chen, H.Q. Preparation and characterization of nanocrystalline titanium dioxide with a surfactant mediated method. *Curr. Nanosci.* **2010**, *6*, 1–5. [[CrossRef](#)]
46. Constable, C.P.; Yarwood, J.; Münz, W.D. Raman microscopic studies of PVD hard coatings. *Surf. Coat. Technol.* **1999**, *116–119*, 155–159. [[CrossRef](#)]
47. Stoehr, M.; Shin, C.-S.; Petrov, I.; Greene, J.E. Raman scattering from  $TiN_x$  ( $0.67 < x < 1.00$ ) single crystals grown on MgO (001). *J. Appl. Phys.* **2011**, *110*, 083503. [[CrossRef](#)]
48. O’Hare, P.A.G. Thermodynamic properties of silicides. III. Specific energy of combustion in fluorine of a hyperstoichiometric disilicide. The standard molar enthalpy of formation  $\Delta_f H_m^\circ$  of  $MoSi_{2.067 \pm 0.002}$  at the temperature 298.15 K. *J. Chem. Thermodynamics* **1993**, *25*, 1333–1343. [[CrossRef](#)]
49. Jehn, H.; Ettenmayer, P. The molybdenum-nitrogen phase diagram. *J. Less Common Met.* **1978**, *58*, 85–98. [[CrossRef](#)]
50. Ee, Y.C.; Chen, Z.; Chan, L.; See, K.H.; Law, S.B.; Xu, S.; Tsakadze, Z.L.; Rutkevych, P.P.; Zeng, K.Y.; Shen, L. Formation of Ti-Si-N film using low frequency, high density inductively coupled plasma process. *J. Vac. Sci. Technol. B* **2005**, *23*, 2444–2448. [[CrossRef](#)]
51. Chi, E.; Shim, J.; Kwak, J.; Baik, H. Silicide formation by solid-state diffusion in Mo/Si multilayer thin films. *J. Mater. Sci.* **1996**, *31*, 3567–3572. [[CrossRef](#)]

**Disclaimer/Publisher’s Note:** The statements, opinions and data contained in all publications are solely those of the individual author(s) and contributor(s) and not of MDPI and/or the editor(s). MDPI and/or the editor(s) disclaim responsibility for any injury to people or property resulting from any ideas, methods, instructions or products referred to in the content.